the film contributes more than 80% of the change of resonant frequency of the AT cut quartz crystal. Hydrogen absorption/desorption and oxidation/reduction of the electrodes can be monitored *in situ* in the discharge and charge period during cycling. The oxide formed during the discharge period can be partially reduced in the charge period.

Acknowledgments

We would like to thank R. Waldo for EPMA. The authors would also like to acknowledge W. J. Meng, F. T. Wagner, D. N. Belton, M. A. Habib, C. L. Dimaggio, T. E. Moylan, and S. J. Schmieg for helpful discussions. We appreciate the continuing support from K. C. Taylor, G. B. Fisher, D. D. Snyder, B. G. Wicke, and S. S. Swathirajan. Y. Li would like to thank the sponsorship from General Motors Corporation for this work which is a part of his Ph.D. research.

Manuscript submitted April 7, 1995; revised manuscript received Aug. 25, 1995.

General Motors Research and Development Center assisted in meeting the publication costs of this article.

REFERENCES

1. M. R. Deakin and O. Melroy, *J. Electroanal. Chem.*, **239**, 321 (1988).
2. S. Butterworth, *Proc. Phys. Soc.*, **27**, 410 (1915).
3. P. L. Konash and G. J. Bastiaans, *Anal. Chem.*, **52**, 1929 (1980).
4. T. Nomura, *Anal. Chim. Acta*, **124**, 81 (1981).
5. T. Nomura and M. Iijima, *ibid.*, **131**, 31 (1981).
6. *Applications of Piezoelectric Quartz Crystal Microbalances*, C. Lu and A. W. Czanderna, Editors, Elsevier, New York (1984).
7. J. Onsgaard and E. Taglauer, *Vacuum*, **34**, No. 10, 1984, p. 831.
8. K. K. Kanazawa and J. G. Gordon, *Anal. Chim. Acta*, **175**, 99 (1985).
9. G. T. Cheek and W. E. O'Grady, *J. Electroanal. Chem.*, **277**, 341 (1990).
10. S. Bruckenstein and M. Shay, *Electrochim. Acta*, **30**, 1295 (1985).
11. Y. Li, Y-T. Cheng, and M. A. Habib, *J. Alloys Comp.*, **209**, 7 (1994).
12. Y. Li and Y-T. Cheng, *ibid.*, **223**, 6 (1995).
13. J. Balej, *Int. J. Hydrogen Energy*, **10**, 365 (1985).
14. Y-T. Cheng and Y. Li, Unpublished results.
15. L Schlapbach, A. Seiler, F. Stucki, and H. C. Siegmann, *J. Less-Comm Met.*, **73**, 145 (1980).
16. E. P. EerNisse, *J. Appl. Phys.*, **43**, 1330 (1972).
17. *Piezoelectric Resonators and Their Applications*, J. Zelenka, Elsevier, New York (1986).
18. T. Sakai, H. Ishikawa, H. Miyamura, N. Kuriyama, S. Yamada, and T. Iwasaki, *ibid.*, **138**, 908 (1991).
19. J. J. G. Willems, *Philips J. Res.*, **39**, 1 (1984).
20. T. Sakai, H. Ishikawa, K. Oguro, C. Iwakura, and H. Yoneyama, *This Journal*, **134**, 558 (1987).
21. N. Yamamoto, T. Ohsaka, T. Terashima, and N. Oyama, *J. Electroanal. Chem.*, **296**, 463 (1990).
22. A. P. M. Glassford, *J. Vac. Sci. Technol.*, **15**, 1836 (1978).
23. R. Beck, U. Pittermann, and K. G. Weil, *This Journal*, **139**, 453 (1992).
24. R. Schumarer, J. G. Gordon, and O. Melroy, *J. Electroanal. Chem.*, **216**, 127 (1987).
25. S. Abe and T. Hosoya, in *Proceedings of the 5th World Hydrogen Energy Conference*, Toronto, ON, Canada, Vol. 4, 1984 (1983).
26. C. Christofides and A. Mandelis, *J. Appl. Phys.*, **66**, 3989 (1989).

Porous Nickel Oxide/Nickel Films for Electrochemical Capacitors

Kuo-Chuan Liu* and Marc A. Anderson**

Water Chemistry Program, University of Wisconsin-Madison, Madison, Wisconsin 53706, USA

ABSTRACT

Nano-sized NiO/Ni composite films have been found to perform as superior electrodes in electrochemical capacitor applications. These films can provide a specific capacitance of 50 to 64 F/g. The specific energy and specific power of these films were 25 to 40 kJ/kg and 4 to 17 kW/kg, respectively. These specific quantities are dependent on the microstructure of the films. Superior performance can be obtained from samples having rough surfaces and consisting of larger secondary particles (*ca.* 100 to 120 nm in diam).

Introduction

Electrochemical capacitors utilize both electrical double-layer and interfacial redox processes to store energy at an electrode/electrolyte interface. The electrical double-layer capacitance of a clean metal surface is in the range of 16 to 30 $\mu F/cm^2$. To make use of electrical double-layer capacitance as a mechanism to store energy, one must produce materials with a high specific surface area. Activated carbon is one example of a material that has been used for this purpose.[1,2] Another material which has been employed in electrochemical capacitors is ruthenium oxide. Ruthenium oxide not only utilizes electric double-layer capacitance as a means to store energy but also exploits pseudocapacitance to enhance this storage capability.[3-5] The pseudocapacitance, *i.e.*, the faradaic oxidation and reduction of an electrode interface or the deposition and removal of a two-dimensional coverage of adatoms on the electrode surface, is potential dependent and highly reversible.[5,6] By combining these two energy-storage processes and by taking advantage of the systems high conductivity, ruthenium-based electrochemical capacitors can offer energy densities about ten times larger and power density 100 times larger than activated carbon-based systems.[6]

For the past decade, much of the research devoted to electrochemical capacitors has been directed at modifying existing material systems in order to enhance their energy and power density. In carbon-based systems, the high internal resistance of the electrode causes the delivery of the stored energy to be relatively slow and therefore poor in power density. To correct this problem, Mayer *et al.*[7] used a high-surface-area carbon aerogel to enhance the power density of carbon-based electrochemical capacitors to 7.8 kW/kg. This represented a tenfold power-density improvement over previous carbon-based electrochemical capacitors. Kohler and co-workers[8] also improved the energy density of carbon-based electrochemical capacitors by using a stainless steel/activated carbon fiber composite. Tanahashi *et al.*[9] achieved a remarkable specific capacitance of 113 F/g from an activated carbon-fiber cloth material (ACFC). Another approach has been to

* Electrochemical Society Student Member.
** Electrochemical Society Active Member.

replace aqueous electrolytes with organic or solid-state electrolytes because such electrolytes can withstand high applied potentials.[10-13] (Cells with aqueous electrolytes are typically limited to potentials of 1 to 1.2 V, whereas organic electrolytes can reach 3 to 4 V.) The benefit of replacing an aqueous with an organic or a solid-state electrolyte lies mainly in an enhancement in energy density. The energy stored in a capacitor is equal to 1/2 CV^2, where C is the capacitance and V is the applied potential. By increasing the working potential, one can increase energy density. However, in solid-state electrolytes one may lose contact with the active materials on the electrode surface, thereby causing a decrease in specific capacitance. Sarangapani *et al.*[13] characterized the RuO_x ionomer composite using both aqueous and solid-state electrolytes. They found about a 40% loss in capacitance in solid-state electrolytes compared to aqueous electrolytes for capacitors employing the same configuration. Also, high internal resistance of nonaqueous systems limits the power density achievable in these systems.

Although RuO_2-based electrochemical capacitors appear to show excellent energy and power densities for many applications, the high cost of this material has retarded its commercial acceptance as an electrochemical capacitor. While carbon-based systems are cheaper, their inherently high internal resistance limits the function of this capacitor only to low-current applications.[2] Therefore, the research community continues to search for new materials and new manufacturing methods for the production of useful electrochemical capacitors. The next generation of electrochemical capacitors must have high conductance (*i.e.*, high conductivity of the electrode and high ionic mobility of the electrolyte in the porous matrix). They must have high specific surface areas. Their electrochemical properties must be characterized as having no bulk redox or self-discharge reactions in the range of applied potential. If possible, surface redox reactions occurring in this range of potential are desired in order to enhance the charge storage capabilities of the capacitor.

In this paper we report on an inexpensive nano-sized NiO/Ni composite electrochemical capacitor (in aqueous KOH solution) which can provide a specific energy of about 25 to 40 kJ/kg and a specific power around 4 to 17 kW/kg based on the mass of NiO/Ni composite. This system offers comparable specific capacitance to the ruthenium oxide and carbon-based systems (30 to 40 F/g), but suffers none of the drawbacks of these two systems. We have found that the microstructure of the composite film controls the specific capacitance of this system.

Experimental

Preparation Methods.—The nickel oxide/nickel composite was prepared from nickel acetate. Nickel acetate tetrahydrate (Aldrich, 95%) is dehydrated at 100 ± 5°C. Ten grams of this dried powder was added to 120 ml Milli-Q water and stirred for two days. The precipitate was separated by centrifugation and resuspended in 5 to 50 ml of Milli-Q water. In this way, two different sols with different volume ratios of the precipitate and water were fabricated to make thin-film samples. The volume ratio of the dilute sol was 1:10, however, the concentrated sol was 1:1. The final solution was opaque having a light green color. Depending on the amount of added water, this solution was stable (if kept at 2 ± 1°C) for 1 to 4 weeks. Fresh opaque solutions with different particle concentrations (described as above) were used to make thin-film samples on 0.125 mm thick nickel foils (Alfa, 99.8%) by using a dipping method with a withdrawal speed of 3.7 mm/s. The film was fired at 300°C for 1 h with a ramp rate of 2°C/min in air. The amount of active material coated on the foil was obtained by subtracting the weight of clean nickel foil from the weight of fired sample. Bulk xerogel samples were obtained by drying the opaque solution at room temperature. These xerogels were fired using the same firing protocol as the thin-film samples (described above). These fired bulk samples were employed to characterize the chemical species, the crystalline phase, and microstructure using infrared spectroscopy (IR), x-ray diffractometry (XRD), and transmission electron microscopy (TEM) techniques.

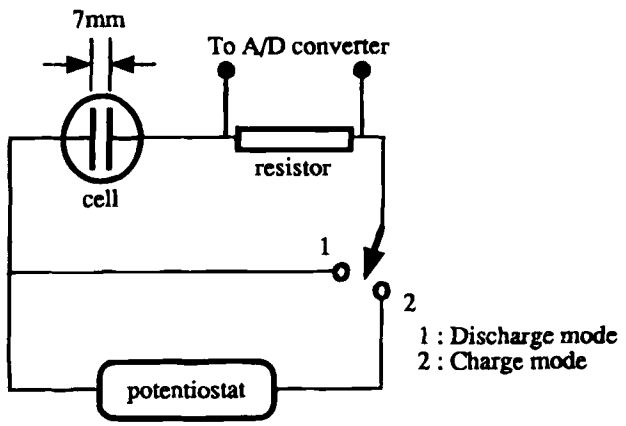

Fig. 1. Schematic representation of the capacitance measurement system.

Capacitance measurements.—Two thin-film samples fixed in a parallel position were immersed in 1 M KOH solution. The space between the two foils was 7 mm. A 100 Ω resistor was placed in series with the test cell. An IBM-PC computer with a Keithley DAS-8 A/D board was used to sample the potential across the 100 Ω resistor every 20 ms. A potentiostat was used to supply a constant potential across the test cell and the resistor while charging. A mechanical switch was used to cut off the potential and turn the circuit into a discharge mode (as shown in Fig. 1). In the discharge mode, the test cell was discharged through the 100 Ω resistor (constant load discharge). Charge and discharge curves were obtained by converting the original data (*i.e.*, the potential across resistor *vs.* time) into current using Ohm's law. The discharge and charge curves were integrated numerically to obtain the total charge stored or released from the cell. The capacitance was calculated by dividing the total charge by the applied potential. The specific capacitance was the capacitance of the cell divided by the weight of active materials (*i.e.*, NiO/Ni films). The specific energy of the capacitor was obtained from equation

$$E = \frac{1}{2}CV^2 \qquad [1]$$

Results

Materials characterization.—The fired bulk samples consisted of a mixed nickel oxide (NiO) and nickel metal (Ni), as illustrated in Fig. 2. From an investigation on the extent of hydrolysis using infrared spectroscopy, we have found that the unfired bulk sample consists of nickel hydroxide and nickel acetate, as shown in Fig. 3. That is, the nickel acetate was partially hydrolyzed.

Microstructural investigation.—The microstructure of the fired bulk sample was investigated using transmission

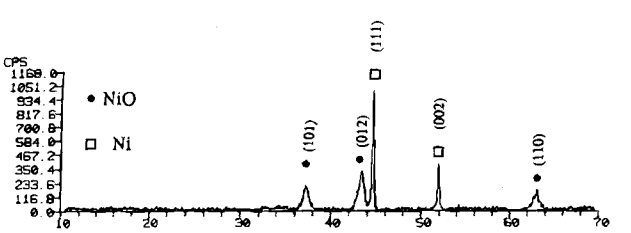

Fig. 2. X-ray diffraction pattern of NiO/Ni sample fired at 300°C for 1 h in air.

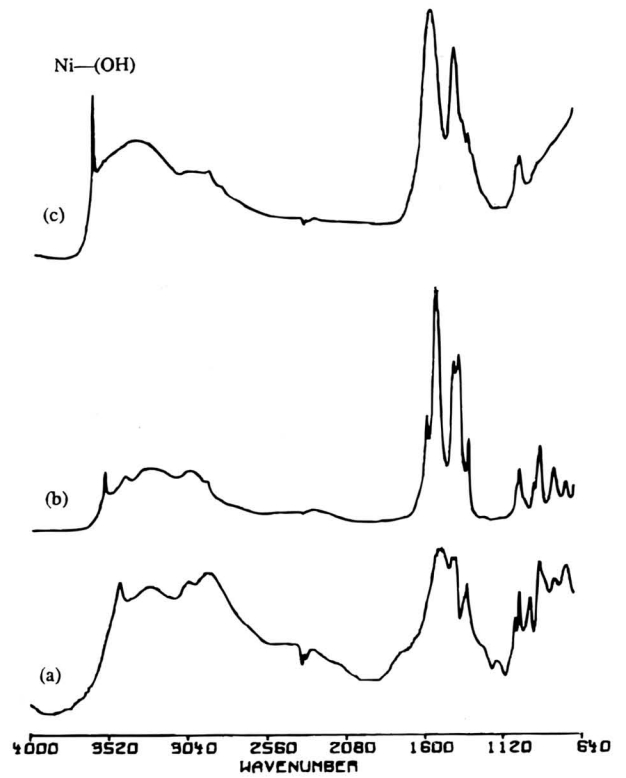

Fig. 3. Infrared spectrum of (a) nickel acetate tetrahydrate, (b) dried nickel acetate tetrahydrate, and (c) unfired bulk sample. It shows the strong Ni-(OH) stretching band at 3645 cm^{-1} in (c). The peaks in the 1120 to 2000 cm^{-1} region belong to the stretching and bending of the atoms in acetate ions.

electron microscopy (JEOL 200CX). This sample had a grain size of *ca.* 3 to 8 nm and a pore size of *ca.* 2 to 3 nm, as shown in Fig. 4. The surface area was characterized by nitrogen sorption Brunauer, Emmett, and Teller method (BET) and found to be 120 m^2/g.

The thin-film samples were shown to have different types of surface morphologies which were dependent upon the concentration of the precursor sols used in coating. As shown in Fig. 5, the sample made from the dilute sol appears to form a well-packed array of smaller particles (*ca.* 10 nm in diam). The roughness of this sample (rms) is 20 nm. In contrast, the sample prepared from a concentrated sol seems to be loose-packed and consists of larger particles (*ca.* 120 nm in diam) and the roughness (rms) is 77 nm. The sample made from the concentrated sol had a specific capacitance of *ca.* 50 F/g, which was two to three times larger than the value of the sample made from the dilute sol.

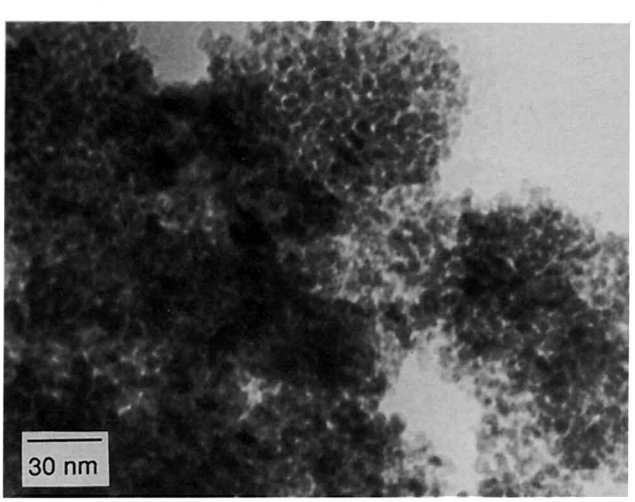

Fig. 4. Transmission electron micrograph of NiO/Ni composite fired at 300°C for 1 h in air.

Electrochemical characterization.—Cyclic voltammetry studies (IBM, EC 225 voltammetric analyzer) were conducted using a pair of electrodes made from a concentrated suspension and performed in a 1 *M* KOH solution using a saturated calomel electrode (SCE) reference electrode. As shown in Fig. 6, the square-like shape is characteristic of electrochemical capacitors. This has been observed in activated carbon and ruthenium oxide systems.[5,6,9] The coulombic efficiencies of these reactions were 0.96 to 0.98, which indicated that this reaction is highly reversible. The differential capacitance calculated from the cyclic voltammogram was about 64 F/g. The potential range is narrow as compared to the potential ranges of the other two materials system. This narrow potential range may limit the obtainable capacitance from this NiO/Ni system. However, the applied potential of a pair of electrodes in bipolar configuration can be as high as 1.8 V without observing apparent decomposition of water. Due to this high applied potential, the energy density of the NiO/Ni system can be higher than the other systems.

An impedance plot (impedance analyzer: HP 4192A) of this system in 1 *M* KOH is shown in Fig. 7. This plot is similar to the impedance of a power transmission line model applied to other electrochemical capacitors.[6] This indicated that this system (*i.e.*, porous NiO/Ni electrodes in 1 *M* KOH solution) had a similar ionic transportation behavior to the carbon or ruthenium oxide systems.

Capacitance measurement.—The charge and discharge curves of the samples prepared from a concentrated suspension for different cycles is shown in Fig. 8. These curves, which are irregular in shape during the first several cycles, become uniform after 10 cycles. The charge and discharge curves can be fit by a resistance-capacitance (RC) model whose discharge and charge curves can be expressed as $I = I_0 \cdot \exp(-t/RC)$. The curve shape changes probably are caused by the variation of the oxidation state of the Ni atoms by the applied potential. Although the gradual wetting of the internal porosity has been considered as the reason, the curve shape changes still existed even if the electrodes were vacuum impregnated with electrolyte or soaked in electrolyte solution overnight. The specific capacitance *vs.* the cycle number is shown in Fig. 9. The high reversibilty of this system can also be demostrated from the close values of the specific capacitance from the charge modes and the discharge modes.

Discussion

Over the past decade, research in the field of electric double layers has held that oxides behave differently than metals with respect to charge development at the solid-liquid interface.[14-18] The surface charge of the oxides is determined by the extent of potential determining H^+ and OH^- ion adsorption. In turn, surface charge is compensated by the counterions in the solution which form the electric double layer at the metal oxide/electrolytic solution interface. This "static" electric double layer is developed within several seconds as the oxide is immersed in the electrolytic solution. Accompanying this chemical adsorption of potential determining ions, a space-charge region develops on the inside of the oxide if the oxide is a semiconductor. The capacitance at the metal oxide/solution interface combines the double-layer capacitance at the solution side and the space-charge capacitance at the oxide side of this interface. In early studies on Li-doped NiO single crystals,[19] both surface charge governed double-layer and space-charge regions were observed in this p-type semiconductor. The capacitance arising from the space-charge region was found to be in the range of 1 to 8 $\mu F/cm^2$ depending on the applied potential.

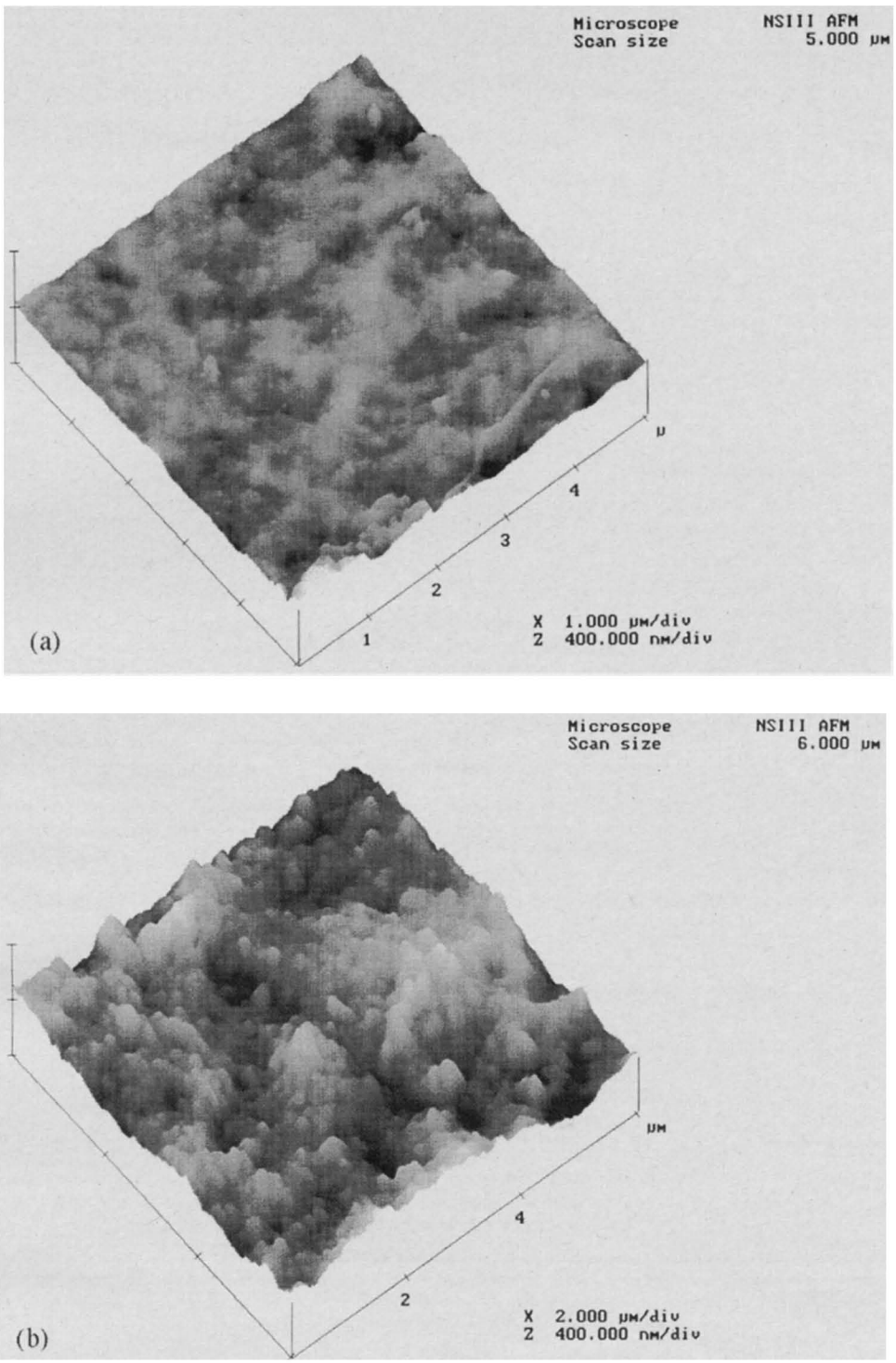

Fig. 5. Surface morphology of NiO/Ni films made from (a) dilute sol and (b) concentrated sol observed by AFM.

The extent of specific adsorption of potential determining ions when governed by the applied potential can be described as the oxidation and reduction of metal ions on the oxide surface. It has been determined that these surface redox reactions may contribute to the measured capacitance over a certain potential range. In recent studies[20,21] on the nonstoichiometric NiO thin films applied as electrochromic devices, it has been shown that the reaction of Ni^{2+} to Ni^{3+}

$$NiO + OH^- \rightarrow NiOOH + e^- \quad [2]$$

occurs at the surface layer of the NiO grain. The series capacitance of this film is also dependent on the applied potential.[20,21] This suggests that the surface redox reaction of NiO contributes to the charge-storage capability of electrochemical capacitors, if the proper physicochemical and microstructural properties are well controlled.

The cyclic voltammogram, impedance spectroscopy, and charge/discharge curves of this system, as illustrated in Fig. 6, 7, and 8, have shown that the characteristics of this system are the same as those existing in electrochemical capacitors. As calculated from the specific surface area and the specific capacitance of this system, the capacitance based on the real surface of this NiO/Ni composite is about 40 to 54 $\mu F/cm^2$. This value is higher than the capacitance from the space-charge region which can be attributed to the exhaustion of holes near the NiO surface[19] (*i.e.*, 1 to 8 $\mu F/cm^2$). It is believed that the pseudocapacitance from the surface adsorption of potential determining ions, the double-layer capacitance in solution, and the capaci-

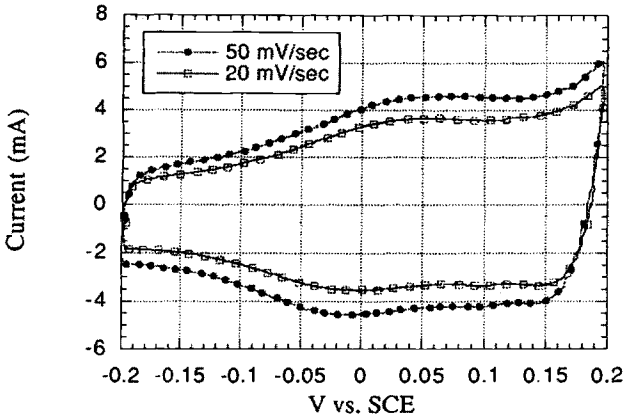

Fig. 6. Cyclic voltammograms of NiO/Ni thin-film electrodes (thickness is around 400 nm) fired at 300°C in 1 *M* KOH at scan rate of 20 and 50 mV/s. The reference electrode is a saturated calomel electrode (+0.2412 vs. the SHE).

tance from the space-charge region contribute to the total capacity of this NiO/Ni composite system.

Early theoretical calculations concerning the stability of colloidal suspension has shown that double-layer repulsion is responsible for the stability of these system Derguin, Landau, Verwey, Overbeek (DLVO theory).[22] In a simplified one-dimensional case, assuming that ions are point charges and their distribution can be represented by Boltzmann distribution, the potential at the middle of two plates in solution can be derived from the Guoy-Chapman model. A schemetic drawing of the interaction of the double layers on two plates is shown in Fig. 10. The middle plate potential ψ_d can be expressed as a function of the distance between two plates

$$e^{\left(-\frac{z-u}{2}\right)} = \cos\left(\frac{\kappa d}{2}\cdot e^{\frac{u}{2}}\right) \qquad [3]$$

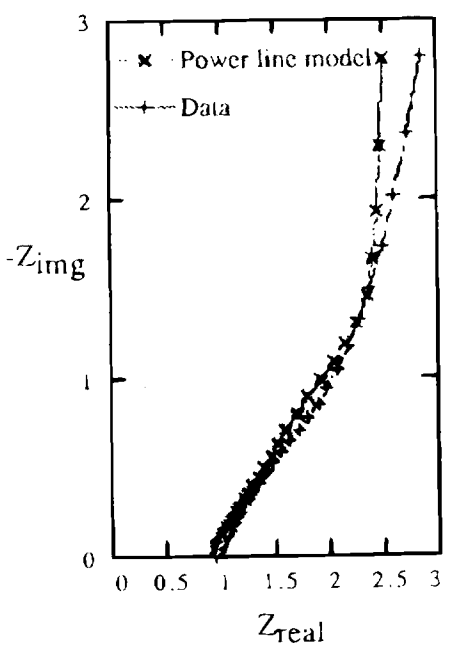

Fig. 7. An impedance plot of NiO/Ni films in 1 *M* KOH with frequency range 5 Hz to 10 kHz.

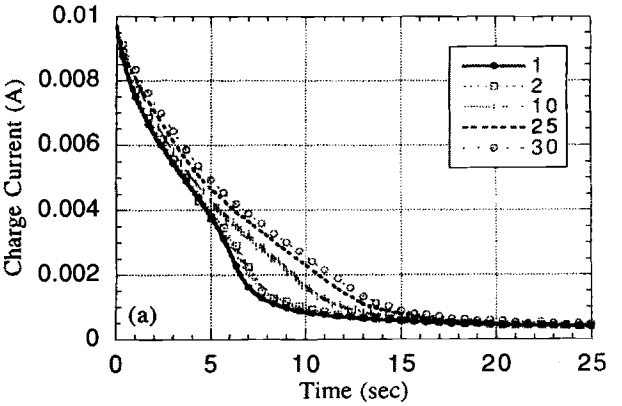

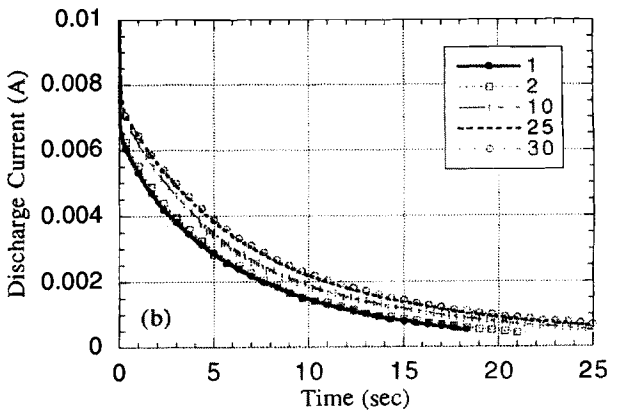

Fig. 8. Charge and discharge curves of NiO/Ni thin-film electrodes in 1 *M* KOH with different cycles; (a) charge curves and (b) discharge curves.

where

$$z = \frac{ve\psi_0}{kT}$$

$$u = \frac{ve\psi_d}{kT}$$

$$\kappa^2 = \frac{8\pi n e^2 v^2}{\epsilon kT}$$

where ψ_0 is the electric potential on solid surface, $1/\kappa$ is the Debye length or thickness of the diffuse layer, $2d$ is the distance between two plates, n is the number of ions per cm^3, v is valence of the ions in electrolyte, and ϵ, k, T, are the dielectric constant of the media, Boltzmann constant

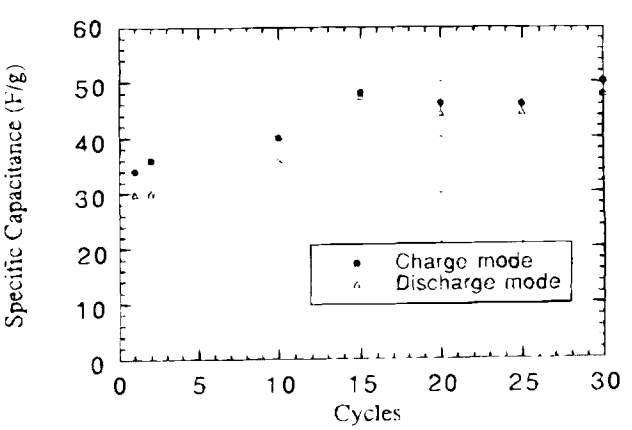

Fig. 9. Specific capacitance of NiO/Ni thin-film electrodes in 1 *M* KOH as function of cycle numbers.

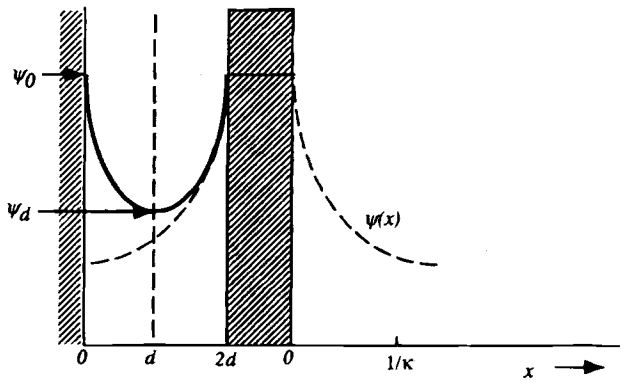

Fig. 10 Schematic representation of the electric double-layer interaction between two plates, in comparison with the potential of a single double layer.

and absolute temperature, respectively. Equation 3 is obtained under the assumption of high surface potential (this assumption is acceptable when the electrolyte concentration is high, such as 1 *M*).The result of Eq. 3 with a surface potential of 0.6 V is shown in Fig. 11.

Figure 11 shows the variation of middle plate potential ψ_d *vs.* the values of one-half of the plate distance, *d*. This figure indicates that as the spacing between two plates becomes smaller, the potential at the center position becomes higher. This phenomenon implies that as the two plates approach each other, fewer ions in solution can enter the space between two plates to compensate for the potential on plate surfaces. Since there are fewer counterions between the two plates, repulsion forces arising from surface charges on the plates will drive them apart. This is the same mechanism which describes the stability of colloidal dispensions. It should be noted that this model does not include the effect of Stern layer adsorption nor does it account for the size of solvated ions. These two factors futher complicate the calculation. A qualitative estimation of the middle plane potential including considerations of Stern layer adsorption and size of solvated ions is drawn schematically in Fig. 11. This simplified model suggests that, in a porous electrode due to the limiting space, a diffuse layer may not develop inside microporous materials. Thus, the total charge stored in microporous electrodes of double-layer capacitors is limited by the capability of developing a diffuse-layer in micropores. Therefore, in constructing electrodes for electrochemical capacitors, one must consider the microstructure of the electrode (*i.e.*, pore size distribution) as an important design parameter. Likewise, for a give microstructure of the electrodes, an optimal electrolyte concentration exists for diffuse layer development.

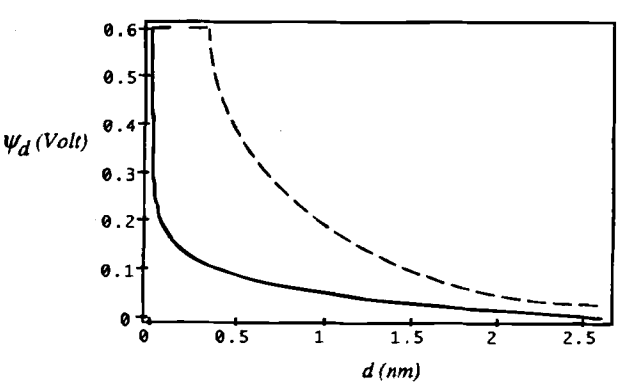

Fig. 11. Potential ψ_d as function of the distance *d* for ψ_0 = 0.6 V, 1 *M* electrolytic solution, and 298 K as calculated from Eq. 3. Dashed line: Schematic drawing of the potential *yd* with consideration of Stern layer and size of solvated ions.

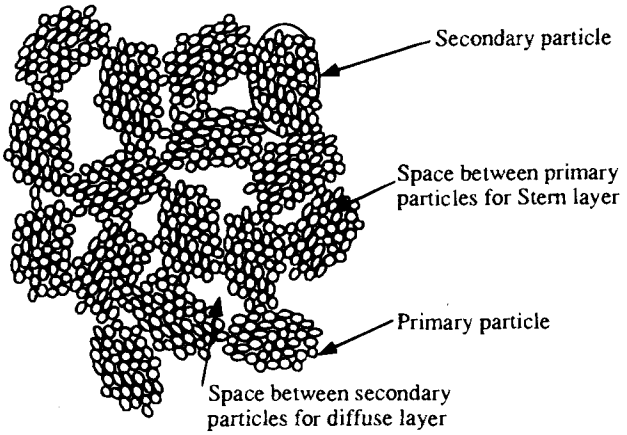

Fig. 12. Schematic representation of the microstructure of the NiO/Ni composite film. The space between nano-sized particles can accommodate the Stern layer. The space between secondary particles can fit not only the Stern layer but also the diffuse layer.

To illustrate this phenomenon we refer to the samples made from dilute and concentrate sols. The surface morphology of these samples as characterized by atomic force microscopy are quite different (Fig. 5). The samples prepared from dilute sols have smooth surfaces and consist of tight-packed array of very small particles (around 10 nm in diam). However, for the samples made from concentrated sols, the roughness of the surfaces is high and the surfaces consist of larger particles (100 to 120 nm in diam). The high roughness of the samples made from the concentrated sol is caused by the agglomeration of the primary particles in solution which provides larger particles and forms a rough surface after firing. These rough surfaces provide enough space for the double layer to develop. This, in turn, provides higher charge storage capability than the smooth surface consisting of nano-sized particles. This has also been demonstrated in the specific capacitance of these samples. In the case of samples prepared from the dilute sol, the specific capacitance is only 18 F/g. However, the specific capacitance of the samples obtained from concentrated sols, which had a rough surface composed of large secondary particles, was 50 F/g. A schematic picture to explain this phenomenon is shown in Fig. 12.

Conclusions

New materials which consist of nano-sized NiO/Ni particles have been found to be good electrochemical capacitors. They can provide a specific capacitance of 50 to 64 F/g, which is in the same range as carbon-based and ruthenium oxide systems reported in the literature.[7,10,13] They also can offer an energy and power density of 26 to 40 kJ/kg and 4 to 17 kW/kg, respectively. These electrochemical capacitors can be prepared from cheap raw materials utilizing simple manufacturing methods. In this system, charge storage is likely due to a combination of surface redox reactions and electrical double-layer developments. The microstructure of this material plays an important role in optimizing the performance of this system. It is believed that loose-packed secondary particles in the film provide a double-layer structure (*i.e.*, a Stern layer and complete diffuse layer) which avoids overlapping interactions. Furthermore, the presence of nano-sized particles and nano-porosity provides a sufficiently large surface area for surface redox reactions to add to the double-layer capacitance of these systems.

Manuscript submitted April 4, 1995; revised manuscript received Sept. 18, 1995.

The Water Chemistry Program at the University of Wisconsin-Madison assisted in meeting the publication costs of this article.

REFERENCES

1. K. Sanada and M. Hosokawa, *NEC Res. Dev.*, **55**, 21 (1979).
2. G. Innocenti and D. Yanko, *Des. News*, **6**, 163 (1986).
3. G. L. Bullard, H. B. Sierra-Alcazar, H. L. Lee, and J. L. Morris, *IEEE Trans. Magn.*, **MG-25**, 102 (1989).
4. S. Sarangapani, P. Lessner, J. Forchione, A. Griffith, and A. B. Laconti, *J. Power Sources*, **29**, 355 (1990).
5. B. E. Conway, *This Journal*, **138**, 1539 (1991).
6. I. D. Raistrick, in *Electrochemistry of Semiconductors and Electronics Processes and Devices*, J. McHordy and F. Ludwig, Editors, Chap. 7, Noyes Publications, Park Ridge, NJ (1992).
7. S. T. Mayer, R. W. Pekala, and J. L. Kaschmitter, *This Journal*, **140**, 446 (1993).
8. D. Kohler, J. Zabasajja, F. Rose, and B. Tatarchuk, *ibid.*, **137**, 1750 (1990).
9. I. Tanahashi, A. Yoshida, and A. Nishino, *ibid.*, **137**, 3052 (1990).
10. I. Tanahashi, A. Yoshida, and A. Nishino, *Denki Kagaku*, **56**, 892 (1988).
11. Y. Matsuda, M. Morita, M. Ishikawa, and M. Ihara, *This Journal*, **140**, L109 (1993).
12. M. Ishikawa, M. Morita, M. Ihara, and Y. Matsuda, *ibid.*, **141**, 1730 (1994).
13. S. Sarangapani, P. Lessner, J. Forchione, A. Griffith, and A. B. LaConti, in *Proceedings of 25th Intersociety Energy Conversion Engineering Conference*, **3**, 137 (1990).
14. D. E. Yates and T. W. Healy, *J.C.S. Faraday 1*, **76**, 9 (1980).
15. J. Lyklema, *Croat. Chem. Acta*, **43**, 249 (1971).
16. H. J. L. Wright and R. J. Hunter, *Aust. J. Chem.*, **26**, 1191 (1973).
17. J. A. Davis, R. O. James, and J. O. Leckie, *J. Colloid Interface Sci.*, **63**, 480 (1978).
18. R. E. Johnson, Jr., *ibid.*, **100**, 540 (1984).
19. T. O. Rouse and J. L. Weininger, *This Journal*, **113**, 184 (1966).
20. D. A. Wruck and M. Rubin, *ibid.*, **140**, 1097 (1993).
21. S. I. Cordoba-Torresi, A. Hugot-Le Goff, and S. Joiret, *ibid.*, **138**, 1549 (1991); *ibid.*, **138**, 1554 (1991).
22. J. W. Verwey and J. Th. G. Overbeek, *Theory of the Stability of Lyophobic Colloids*, Elsevier Publishing, New York (1948).

Electrodeposition of Nickel-Aluminum Alloys from the Aluminum Chloride-1-methyl-3-ethylimidazolium Chloride Room Temperature Molten Salt

William R. Pitner* and Charles L. Hussey**

Department of Chemistry, University of Mississippi, University, Mississippi 38677, USA

Gery R. Stafford**

National Institute of Standards and Technology, Materials Science and Engineering Laboratory, Gaithersburg, Maryland 20899, USA

ABSTRACT

The electrodeposition of nickel and nickel-aluminum alloys on glassy carbon was investigated in the 66.7-33.3 mole percent (m/o) aluminum chloride-1-methyl-3-ethylimidazolium chloride molten salt containing electrogenerated nickel(II) at 40°C. The electrodeposition of nickel on glassy carbon involves three-dimensional progressive nucleation on a finite number of active sites with hemispherical diffusion-controlled growth of the nuclei. At potentials slightly more negative than those needed to induce the reduction of nickel(II) to the metal, aluminum is codeposited with nickel to produce Ni-Al alloys. Controlled-potential and controlled-current experiments revealed that it is possible to produce alloy deposits containing up to approximately 40 atomic percent (a/o) aluminum under conditions that circumvent the bulk deposition of aluminum. The aluminum content of the Ni-Al deposit was found to vary linearly with the deposition potential but nonlinearly with the current density. The electrodeposited Ni-Al alloys are thermodynamically unstable with respect to nickel(II), *i.e.*, immersion of the alloy deposit in melt containing nickel(II) under open-circuit conditions leads to a reduction in the aluminum content of the alloy. The mechanism of alloy formation appears to involve underpotential deposition of aluminum on the developing nickel deposit; however, alloy formation must be kinetically hindered because the aluminum content is always less than predicted from theoretical considerations. Ni-Al alloys produced at 0.30 V [*vs.* Al/Al(III) in pure 66.7-33.3 m/o melt] in melt containing nickel(II) and 20% (w/w) benzene as a cosolvent contained about 15 a/o nickel and were of high quality with a disordered fcc structure, but alloys produced at more negative potentials had the visual appearance of a loosely adherent, finely divided, black powder and were heavily contaminated with chloride, probably as a result of the occlusion of the molten salt solvent by the dendritic alloy deposit during deposit growth.

Introduction

The electrodeposition of aluminum or aluminum alloys from aqueous solutions is complicated by the fact that hydrogen is evolved before aluminum is deposited. Thus, aprotic nonaqueous solvents or molten salts must be used to electroplate these materials. The electrodeposition of a number of transition metal-aluminum alloys such as Cr-Al,[1] Mn-Al,[2] Ni-Al,[3] and Ti-Al[4] has been demonstrated from inorganic chloroaluminate molten salts, mainly Lewis acidic or $AlCl_3$-rich $AlCl_3$-NaCl. One unfortunate drawback to the use of alkali-chloride based chloroaluminates such as this for the electroplating of these alloys is the substantial vapor pressure of Al_2Cl_6 associated with the acidic composition region of these melts (>1.3×10^4 Pa at 154°C). This is inconvenient for most technological applications.

Organic chloroaluminates, which are obtained when certain anhydrous organic chloride salts such as 1-(1-butyl)pyridinium chloride (BupyCl) or 1-methyl-3-ethylimidazolium chloride (MeEtimCl) are combined with $AlCl_3$, are viable alternatives to the inorganic chloroaluminates mentioned above because they can be employed at or close to room temperature, and they exhibit negligible vapor pressure at elevated temperatures. The physical, chemical, and electrochemical properties of these molten salts have been reviewed at length.[5,6]

* Electrochemical Society Student Member.
** Electrochemical Society Active Member.